Discriminant Color Texture Descriptors for Diabetic Retinopathy Recognition

Holly H. Vo and Abhishek Verma
Department of Computer Science
California State University
Fullerton, California
Email: hhvo, averma@csu.fullerton.edu

***Abstract*—Diabetic retinopathy (DR) is a common eye disease that could lead to irreversible vision loss but hard to be noticed by carriers in early stages. Instead of isolating DR signs for DR recognition, this paper examines discriminant texture features obtained by color multi-scale uniform local binary pattern (LBPs) descriptors on five common color spaces and two proposed hybrid color spaces. The extracted features are evaluated by the enhanced Fisher linear discriminant, EFM. Experiments are done on a large dataset of 35,126 training images and 53,576 testing images that have been taken by different devices with high variance in dimensions, quality and luminance. The best performance is above 71.45% by HSI-LBPs, a*SI-LBPs, and bSI-LBPs descriptors.**

***Index Terms*—diabetic retinopathy recognition, DR, texture, uniform LBPs, EFM, FLD, PCA, color space**

I. Introduction

According to US Center for Disease Control and Prevention, diabetic retinopathy (DR) is the most common eye disease which affects one in three Americans with diabetic and further leads to blurred vision and blindness. DR is caused due to high blood glucose level which damages small blood vessels in retina. In consequence, blood, extra fluid, cholesterol, and other fats leak in the retina and make the macula swollen and thicken. Damaged capillaries may finally close and stop providing nutrients and oxygen to retina. To supply sufficient blood to the area, the retina grows new abnormal fragile blood vessels called intraretinal microvascular abnormalities (IrMAs); however, the new vessels are usually accompanied with scar tissue which may wrinkle or detach the retina and distort vision. In late stages, increased pressure in eye may damage the optic nerve [1].

Unfortunately, DR carriers do not notice vision changes in the early stages. DR usually affects both eyes and causes irreversible vision loss in many cases as DR progresses while detecting early DR stages and timely treatment can reduce the risk of severe vision loss by over 90%. Currently, detecting DR is a time-consuming manual procedure which requires ophthalmologists to evaluate digital fundus photography, review, and follow up in many days and causes delayed treatment [2], [3].

A typical fundus image appears with an optic disc, blood vessels, and a macula. Macula is the center area of the retina which contains color-sensitive rods and the central point of sharpest vision. Figure 1 illustrates a fundus image with labeled signs of diabetic retinopathy. Microaneurysms (MAs) are tiny bulges in blood vessels and appear as deep-red dots in the fundus. Haemorrahages are small spots of blood discharge. Hard exudates are leakage of lipid and protein in the retina. Hard exudates typically emerge as bright, reflective, white or cream lesions. Hard exudates and microaneuryms around macula might block vision and additionally damage the macula and leads to permanent vision loss [3], [4].

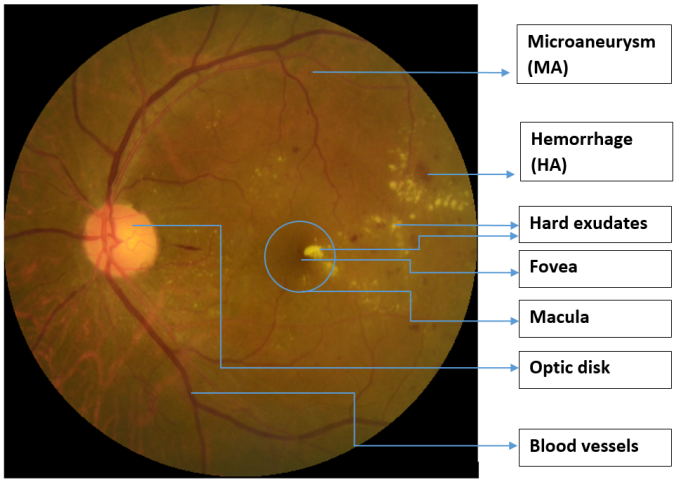

Fig. 1. DR signs and main structure in a retina image

By examining patient retina images, an ophthalmologist can identify two types of retinopathy: nonproliferative diabetic retinopathy (NPDR) and proliferative diabetic retinopathy (PDR). NPDR is further classified into three stages based on the presence of DR signs. Mild NPDR is formed when some microaneurysm appears with possible appearance of exudates and venous loops. Moderate NPDR is developed with multiplex microaneuryms, haemorrhages, and hard exudates. Severe NPDR stage is characterized by 4-2-1 rule. The 4-2-1 rule is defined by the existence of hemorrhages and microaneurysms in four quadrants, venous beading in two quadrants, and IrMAs in one quadrant. Finally, PDR is the advanced stage where new fragile blood vessels leak hemorrhages and hard exudates into the vitreous, the gel in the center of the eye, deliver scar tissue and wrinkle to the retina, build up pressure in the retina, and lead to vision loss due to the damage of macula and optic nerve [3], [5].

This paper is a focus on robust discriminant texture features on color spaces for a large-scale dataset. The rest of the paper is organized as follows. Section II reviews background of current feature extraction and classification techniques on DR. Section III describes the retina image dataset in this research. Section IV proposes the methodology to extract color texture features and classification techniques to identify DR stages. Experimental results and discussion present in section V. Section VI concludes the research with future direction.

II. Related Work

With the clinical fact that MAs are the earliest signs of diabetic retinopathy [6], most DR papers focus on extracting clinical features by localizing and segmenting lesions, blood vessels, optic disks, and macula one by one. Basic point operators are applied to balance and enhance local contrast, and linear filters and neighborhood operators such as morphological operators, median filters, and Gaussian filters are convoluted on images in pre-processing as indicated in surveys [3], [7]. Watershed transformation is applied in [8] to overcome over-segmentation caused by thresholds. Other techniques such as active contour models and recursive region-growing technique (RRGT) are used in the domain researches to isolate blood vessels and other interested regions [7].

In addition to segmentation, statistical texture extraction is another approach in DR recognition. Statistical texture approach is based on the relationship between pixel intensities. In statistical approach, entropy, contrast, and correlation can be simply calculated via gray level co-occurrence matrix. Contrast texture is extracted together with isolated areas of MAs and HAs in [9] to classify DR. In recent years, local binary pattern (LBP) texture is started being used for DR detection on small retina datasets with less than 100 images in [10], [11]. In other domains such as face and scene recognition, texture descriptor such as local binary pattern texture has been proven to contribute significant performance [12].

When sampling on a large set of images which are taken by different devices under various conditions of light and intensity, it is crucial for a robust vision system to adapt a discriminant color space. HSI is applied for Messidor and DB-rect DR datasets in [1] to extract MAs and exudates, and selected by [13] to locate fovea. Green component in RGB is focused to extract blood vessel structure in [9], [14]. All channels of RGB are separately examined in [5] with morphology operations to extract the total area and perimeters of blood vessels, HAs, and MAs. Ram and Jayanthi [15] consider multiple color spaces such as RGB, L*u*v*, HSV and HSI to extract lesion pixel values.

In general, the aforementioned researches focus on segmentation of blood vessels and DR signs for feature extraction on small datasets whose sizes are ranging from several hundreds to several thousands of images. In classification stage, support vector machine (SVM) and artificial neural network (ANN) are two popular techniques in DR problems [1], [5], [7], [9]–[11], [14]. An SVM classifier transforms the original training data to a higher dimension space where it can find a linear optimal separating hyperplane. Meanwhile, multi-layer NN is built on a set of connected input and output nodes and weighted connections between nodes. The network is trained in iterations to determine the proper connection weights, and its back propagation algorithm searches for a set of weights by gradient descent method [16]. Acharya et al. [14] applies SVM on a dataset of 331 retina images to identify five DR stages with an overall accuracy of 86%. Back propagation neural network is applied in [5] with one hidden layer to identify four DR stages with an accuracy of 84% on a dataset of 124 images.

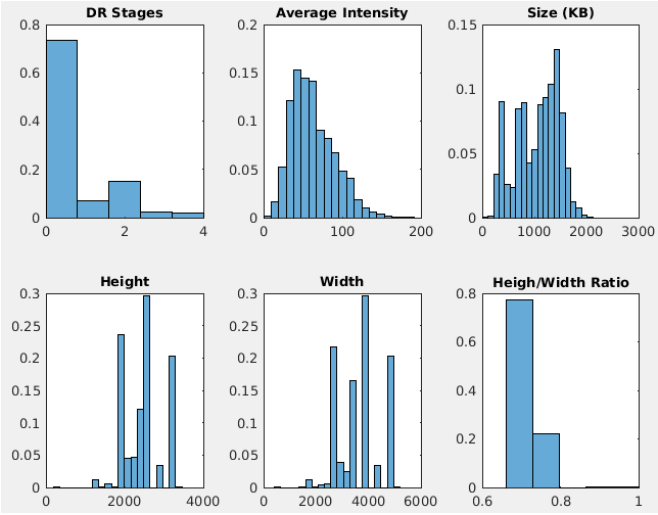

Fig. 2. Statistics of DR training dataset

III. Retinopathy Image Dataset

In this paper, experiments are done on the retinopathy image dataset provided by EyePACS, a free platform for retinopathy screening, through Kaggle website. The dataset originally consists of 35,126 training images and 53,576 testing images. These images are taken by different models and types of camera under different conditions and stored in various, high resolutions. Each image has been examined on the presence of DR by a clinician to be labeled with a DR stage from 0 to 4, corresponding to no DR, mild, moderate, severe, and proliferative DR as being described in the introduction section. Within the train dataset, there are 74% images of stage 0 (no DR), 7% of stage 1 (mild), 15% of stage 2 (moderate), 2% of stage 3 (severe) and 2% of stage 4 (proliferate DR) approximately. Images in the test datasets are split to 5 stages in the similar ratios as in the train dataset.

The challenges of this dataset are its large variance in resolution, intensity, and quality as shown in Figure 2. By examining the train dataset, image heights vary from 289 to 3456 pixels, while their widths vary from 400 to 5184 pixels with the range of ratios between height and width is from 0.66 to 1.00. The average of image intensity spreads from 1 to 192 around the mean of 63. Low intensity images are stored in 8KB while other images can allocate up to 2MB files.

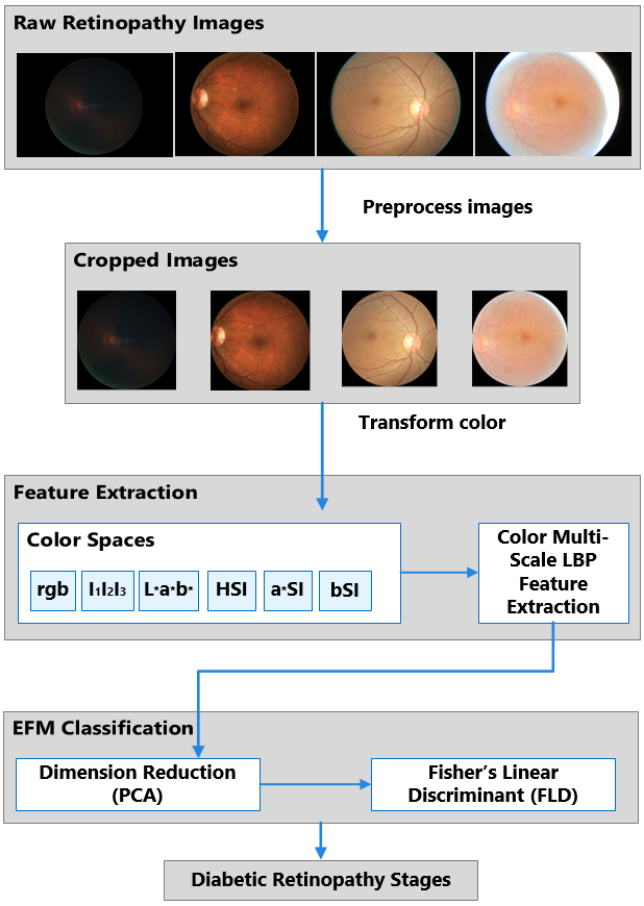

Fig. 3. Methodology Overview

IV. Algorithm Description

In this work, we examine DR classification performance by extracting uniform LBP features at multiple scale on commonly used color spaces such as RGB, HSI, L*a*b*, rgb, and $I_1I_2I_3$, and two hybrid color spaces a*SI and bSI. The proposed method consists of three major parts: image preprocessing, feature extraction on a color space, and classification via an enhanced Fisher model (EFM) built upon principal component analysis (PCA) and Fisher's linear discriminant method (FLD).

A. Image Preprocessing

As being mentioned in dataset description section that input images are in a large range of dimension, the main goal of image is converting any input image of any size to a fixed square image, whose dimension is also the diameter of the circular eye shape. For a given image, a circumscribing rectangle of the eye is determined by scanning pixels along the horizontal and vertical mid-lines of the image from the image boundary toward its center until obtaining an intensity difference above a small threshold. The image is then cropped around the center of the determined circumscribing rectangle to extract a square image whose dimension is the shorter side of the boundary rectangle. Next, the square image is scaled by bicubic interpolation method to a 512x512 image before being clipped around its center by a radius r=256 to guarantee that retina content is captured in a full inscribed circle of the final output square image.

In preprocessing part, training images in DR stages 1-4 are also increased by flipping and rotation to balance training image quantities for all DR stages and avoid over-train on stage 0. Let p_i be the distribution of stage i in the training dataset, where $i = 0..4$ and $\sum_{i=0}^{4} p_i = 1$. To balance with the dominant image population in non-DR stage (0), images in stage i are flipped to double their class size to $2 * p_i$ and then rotated sequentially around their centers by an angle $\alpha_j = j * \lfloor \frac{360^0}{\lceil p_0/(2*p_i) \rceil} \rfloor$, where $j = 1..\lceil p_0/(2 * p_i) \rceil - 1$.

B. Feature Extraction

1) Color Spaces: Colors are wavelengths of light that are reflected by object surfaces and perceived by human eyes. A color space is a mathematical model to organize colors in a way that relates to the perceived colors. Each color space possesses specific characteristics with different discriminating power and suitable for selective visual tasks. The fundamental RGB color space is built on three primary color components close to red, green, and blue wavelengths and used in reproduction systems [17]. In gray scale, intensity is obtained by a weighted sum of red, green, and blue components:

$$I = 0.299R + 0.587G + 0.114B \tag{1}$$

The $I_1I_2I_3$ color space is obtained by the decorrelation of RGB color components through Karhumen Loéve [18]. The color space was found in 1980 in the experiments of region segmentation. The color components are ordered by their segmentation effectiveness and formed by the following transformation:

$$\begin{aligned} I_1 &= \frac{R+G+B}{3} \\ I_2 &= \frac{R-B}{2} \\ I_3 &= -\frac{G+B}{2} \end{aligned} \tag{2}$$

The rgb color space is a chromaticity space defined by normalizing RGB components to reduce the sensitivity of luminance [19]. The color space is represented by the proportion of red, green, and blue in the original RGB color space:

$$\begin{aligned} r &= \frac{R}{R+G+B} \\ g &= \frac{G}{R+G+B} \\ b &= \frac{B}{R+G+B} \end{aligned} \tag{3}$$

With the original aim of representing colors in reproduction system, RGB is device dependent and not intuitive to human vision. Thus, perceptual color spaces are created by relating components in RGB color space to colors characteristics such as hue, brightness, and saturation to facilitate human

interpretation of their components [17]. HSI is a perceptual color space whose components approximate the perceived hue, saturation, and intensity in order. HSI components are obtained by the following equations:

$$\begin{aligned} H &= \begin{cases} \alpha, & \text{if } b < g \\ 2\pi - \alpha, & \text{otherwise} \end{cases} \\ S &= 1 - min(r, g, b) \\ I &= \frac{R + G + B}{3} \end{aligned} \tag{4}$$

where

$$\alpha = cos^{-1}\left\{\frac{0.5 * [(r-g) + (r-b)]}{[(r-g)^2 + (r-b)(g-b)]^{1/2}}\right\}$$

and r, g, and b are normalized RGB components obtained by equation 3.

CIE XYZ color system was defined by the Commission International de L'Eclairage (CIE) in 1931. While RGB uses visible physical colors, XYZ is built upon imaginary primary colors [X Y Z] to form a device-independent color space with better descriptive properties [17]. A color space defined in this system, referred to as Yxy, can represent all visible color by only positive normalized mixture of its primaries and the luminance value Y:

$$\begin{aligned} x &= \frac{X}{X + Y + Z} \\ y &= \frac{Y}{X + Y + Z} \\ z &= 1 - x - y \end{aligned} \tag{5}$$

L*a*b* can be directly derived from XYZ with the intention to mimic the logarithmic response of the human vision system. The L* channel represents luminance in the range from 0 to 100, while a* and b* channels represent chrominance opponents. The red and green opponent colors are represented along a* dimension. The yellow and blue opponent colors are represented along the b* dimension. L*a*b* is widely used in many industries which requires accurate color specifications such as paint, dyes, and printing inks [20]. L*a*b* components can be derived from XYZ as the following:

$$\begin{aligned} L^* &= 116 f(\frac{Y}{Y_n}) - 16 \\ a^* &= 500[\frac{X}{X_n} - \frac{Y}{Y_n}] \\ b^* &= 200[\frac{Y}{Y_n} - \frac{Z}{Z_n}] \end{aligned} \tag{6}$$

where

$$f(t) = \begin{cases} t^{(1/3)} & \text{if } t > (\frac{6}{29})^3 \\ \frac{1}{3}(\frac{29}{6})^2 t + \frac{4}{29} & \text{otherwise} \end{cases}$$

and X_n, Y_n, and Y_n are the CIE XYZ component values of the reference white point.

Table I. Sample images in different color spaces

Color Space	sample images in different stages				
	no DR (0)	mild NPDR (1)	moderate NPDR (2)	severe NPDR (3)	PDR (4)
RGB	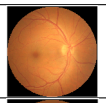				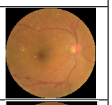
rgb	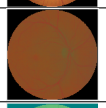	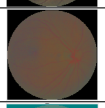	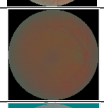	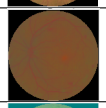	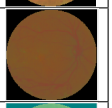
$I_1I_2I_3$	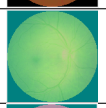	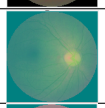	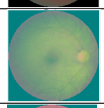	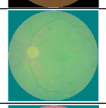	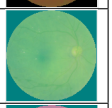
L*a*b*					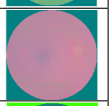
HSI	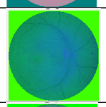	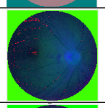	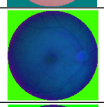	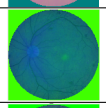	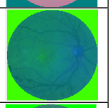
a*SI	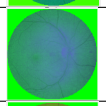	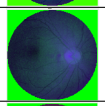	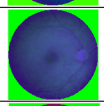	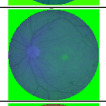	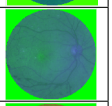
bSI	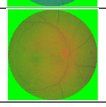	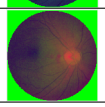	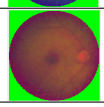	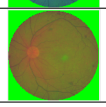	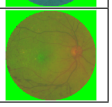

a) Proposed Hybrid Color Spaces: In addition to the existing color spaces, experiments are similarly conducted on two hybrid colors that are derived from HSI: a*SI and bSI. The only difference between the hybrid colors and the original color space HSI is the first channel. The first channel of a*SI is the a* channel of L*a*b*, and the first channel of bSI is the normalized blue channel of rgb.

For a sample retina image of each DR stages, the transformed image corresponding to the discussed color spaces in this section are displayed in Table I.

2) LBP Features: The local binary pattern (LBP) texture descriptor was proposed and improved by Ojala et al. [21], [22]. LBP has been proven as a robust feature descriptor for texture classification [19], [23]. LBP is particularly applied in biometrics, face detection and recognition, and scene recognition [19], [23].

The basic LBP focuses on each 3x3 neighborhood to form an ordered 8-bit LBP code by comparing the surrounding pixels' gray value with its center. The local binary pattern around a pixel P by eight neighbor P_x is encoded as follows:

$$\begin{aligned} LBP &= \sum_{x=1}^{8} s(x) 2^{x-1} \\ s(x) &= \begin{cases} 1 & \text{if } P_x > P \\ 0 & \text{otherwise} \end{cases} \end{aligned} \tag{7}$$

As the operator focuses on the signed differences of gray values and disregards the value difference, it is invariant to changes in mean luminance. For scale invariance improvement, LBP operator is extended to consider a circularly symmetric neighbor set of P pixels on a circle of radius R surrounding the center pixel, denoted as $LBP_{P,R}$. The top middle neighbor is the most significant bit in LBP code, and other neighbors are ordered clockwise. For each neighbor point whose coordinators are not exactly in the center of pixels, its gray value is estimated by interpolation rather than the nearest pixel's value.

The extension in [22] defines a so-called *uniform pattern*, denoted as $LPB^{riu2}_{P,R}$, which contains at most two spatial transitions in its circular chained binary pattern, "1-0" and "0-1". $LPB^{riu2}_{P,R}$ does not only improve rotation invariance but also significantly reduces LBP dimension by preserving a single bin for all nonuniform patterns.

In the real diabetic retinopathy recognition problem, images are taken by different devices under different conditions of light and quality. In addition, besides the main structure of a retina in the images, DR signs are fine-grain and their granularity diversifies. Recall that microaneurysms (MAs) are tiny red dots, hemorrhages and hard exudates can be at any size in any unknown shape, and fragile blood are developed in undetermined directions. Thus, uniform local binary pattern detection should be applied on different scales to capture discriminant features that are invariant to rotation, global intensity, and scales.

In our experiments, each 512x512 retina image is divided into four regions. Texture features are extracted on 4 scales by $LPB^{riu2}_{8,2}$, $LPB^{riu2}_{16,4}$, $LPB^{riu2}_{24,6}$, and $LPB^{riu2}_{32,10}$ descriptors on each 256x256 region at each color channel for a given color space. The extracted LBP features are standardized on each scale. The final 1056-dimension feature vector for a color retina image is formed by standardizing the concatenation of 120 features from $LPB^{riu2}_{8,2}$, 216 features from $LPB^{riu2}_{16,4}$, 312 features from $LPB^{riu2}_{24,6}$, and 408 features from $LPB^{riu2}_{32,10}$.

C. EFM Classification

The extracted LBP features on a color space will be classified by the Enhanced Fisher Model (EFM), which enhances Fisher Linear Discriminant (FLD) by principal component analysis (PCA) [12], [19], [25].

Let X be a data matrix which consists of M feature vectors, X_i, in the space R^N, where $i = 1..M$. The feature vector X_i may reside on a high dimensionality space. The vector is probably composed of correlated features and contains noises. PCA is a common technique to linearly transform data to a lower dimensionality space and reduce data noise [24]. The basic idea of PCA is diagonalizing the covariance matrix, Σ_X, of the original space, R^N, to obtain eigenvectors.

$$\begin{aligned} \Sigma_X &= \mathcal{E}\{[\mathcal{X} - \mathcal{E}(\mathcal{X})][\mathcal{X} - \mathcal{E}(\mathcal{X})]^t\} \\ \Sigma_X &= \Phi \Lambda \Phi^t \end{aligned} \tag{8}$$

where $\mathcal{E}(X)$ is the expectation function, t denotes matrix transpose operation, $\Phi = [\phi_1, \phi_2, \ldots \phi_N]$ is the orthogonal eigenvector matrix, and $\Lambda = diag\{\lambda_1, \lambda_2, \ldots, \lambda_N\}$ is the diagonal eigenvalue matrix in the descending order of eigenvalues.

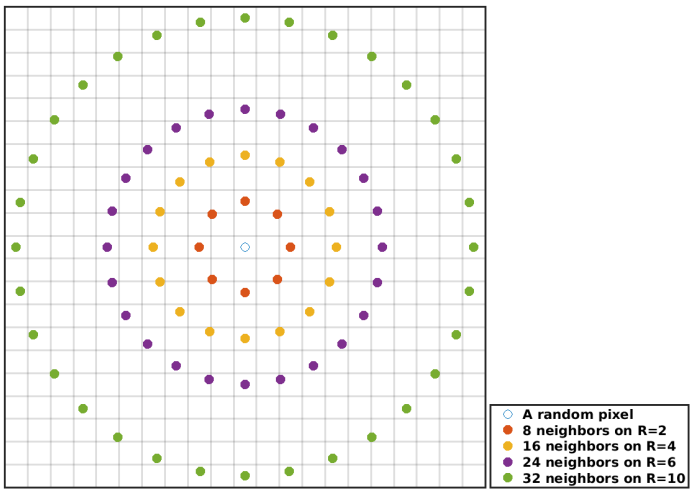

Fig. 4. (8,2), (16,4), (24,6), and (32,10) LBP neighborhoods

A corresponding feature vector, Y_i, in the PCA reduced space, R^K, where $K < N$, is composed by K most dominant principal components and is derived by the following equation:

$$Y_i = P^t X_i \tag{9}$$

where $P = [\phi_1, \phi_2, \ldots, \phi_K]$.

Although PCA is a popular technique in pattern recognition, it is not optimized for class separability. Instead, the alternative technique, FLD, has been proposed to model the difference between classes of data [25], [26].

The Fisher linear discriminant (FLD, a.k.a. linear discriminant analysis LDA) is a popular discriminant criterion that defines a projection to reduce within-class scatter and enlarge the between-class scatter [25]. Let ω_i, where $i = 1..L$, represent the i-th class in a domain, $P(\omega_i)$ and M_i be its corresponding $priori$ probability and mean respectively, and M be the grand mean. The within-class and between-class scatter matrices, S_w and S_b, are defined as

$$\begin{aligned} S_w &= \sum_{i=1}^{L} P(\omega_i)\mathcal{E}\{(\mathcal{Y} - M_i)(\mathcal{Y} - M_i)^t | \omega_i\} \\ S_b &= \sum_{i=1}^{L} P(\omega_i)(M_i - M)(M_i - M)^t \end{aligned} \tag{10}$$

where S_w, $S_b \in R^{mxm}$, $m < N$ and $m < L$.

Let Ψ be a projection matrix. FLD method aims to optimize the ratio $|\Psi^t \Sigma_b \Psi| / |\Psi^t \Sigma_w \Psi|$, which represents the class separability in the domain. The maximized ratio is achieved when Ψ consists of eigenvectors of the matrix $S_w^{-1} S_b$ [25]

$$S_w^{-1} S_b \Psi = \Psi \Delta \tag{11}$$

where Δ are the eigenvalues of the matrix $S_w^{-1} S_b$.

The FLD method encounters overfitting drawback when there are insufficient sample data for generalization. The

Enhanced Fisher model, EFM, overcomes this issue by combining PCA and FLD in the proper balance of the selected eigen features for an adequate representation of raw data and the requirement that the eigenvalues of the within-class scatter matrix in the reduced PCA are sufficient large for generalization [12].

In EFM classifier, discriminant features, Z, are obtained by projecting the PCA reduced feature vectors Y, which are derived in Eq. 9 on the optimal projection matrix Ψ. Each discriminant feature is assigned to the nearest class by measuring its cosine distances to all class centers in our experiments.

$$Z = \Psi^t Y \tag{12}$$

$$\delta_{cos}(x, y) = -\frac{x^t y}{||x||||y||} \tag{13}$$

In this work, EFM is selected for DR recognition experiments on multiple colors and color channels for its simplicity in terms of computation and parameters and its proven effectiveness in the domain of face recognition. Because of the small number of classes in DR recognition experiments, the maximum FLD feature dimension, $m = L - 1 = 4$, is chosen for the best generalization of within and between class relationship. The balanced PCA criterion for the selected FLD feature dimension is determined by 5-fold cross-validation on the train dataset. For validation, the train dataset is equally divided into five folds. Each fold is sequentially tested by the EFM classifier trained on the remaining data. The optimal PCA criterion obtained in validation will be applied to train the final EFM classifier on the whole train dataset in the each experiment.

V. Experiment Results

Experiments are initially conducted on gray scale and five different color spaces. The performance is measured by the correct classification rate on the test dataset. Experiment results obviously show that all color spaces surpass gray scale performance. Among examined color spaces, intuitive color space L*a*b* and HSI outperforms RGB, rgb, and $I_1I_2I_3$. The multiscale LBP descriptor on HSI, denoted as HSI-LBPs, achieves the best performance, 71.45%, among the five descriptors, and it exceeds gray scale by 5.47%. The results support the idea of selecting HSI as the color space to extract MAs and exudates in [1]. It is apparent to understand that the rgb color space performs worst (66.30%) due to the complete absence of luminance. Performance on the proposed hybrid color spaces, a*SI and bSI, is 71.49%, that is slightly better than HSI performance as summarized in Figure 5. Figure 6 shows some RGB images that are not correctly classified by RGB-LBPs and Lab-LBPs descriptor but correctly classified by HSI-LBPs, aSI-LBPs, and bSI-LBPs descriptors. One can visually realize that these example images are very different in terms of light and color.

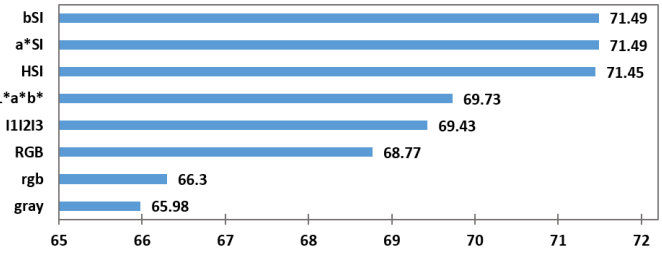

Fig. 5. Total classification performance on color spaces

Table II. LBP-EFM performance on color channels

	Color Space	Channel 1	Channel 2	Channel 3
HSI	71.45	65.92	68.79	65.93
L*a*b*	69.73	66.03	63.69	61.18
I123	69.43	65.93	62.21	61.99
RGB	68.77	63.98	65.64	61.73
rgb	66.30	61.59	61.05	60.50
gray	65.98	65.98		

For more insights on color LBPs descriptors, experiments are further carried on individual channels of each aforementioned color. In rgb color space, b channel performs worst. The best performance, 61.59%, on the r channel is only 1% above the worst channel but 5% below the performance of the color space. It means that different discriminant features could be arranged on every channel of rgb, thus, there is no significantly strong channel and rgb significantly outperforms its individual channels.

In the other four color spaces, improvement of each color performance over its best channel is not as significant as in rgb. The performance improvement on these color spaces is from 2.7% to 3.8%. There is a dominant channel that outperforms the worst channel from 2.9% to 3.9% in each color space. In RGB, green channel achieves the best performance and this result could explain why it is the selected channel to extract blood vessel structure in [9], [14]. The first channel of $I_1I_2I_3$ performs better than other two channels because it the channel holding most chrominance and luminance information. In L*a*b* color space, the luminance channel L* outperforms chrominance channels.

In HSI and proposed HSI-like hybrid color spaces, the most discriminant features are identified on the saturation channel. Although intensity and hue performs at the same rate, a* and b channels performance is at least 2% less than hue. It could be implied that there are more discriminant features that are not found in saturation channel could be identified in channel I than in channel H. It should be noticed that channel I of HSI is also the strongest channel of $I_1I_2I_3$.

VI. Conclusion

We have introduced in this paper different color multi-scale local binary pattern texture descriptors, LBPs, for diabetic retinopathy recognition on a large dataset. The enhanced Fisher linear discriminant is applied to identify the promising

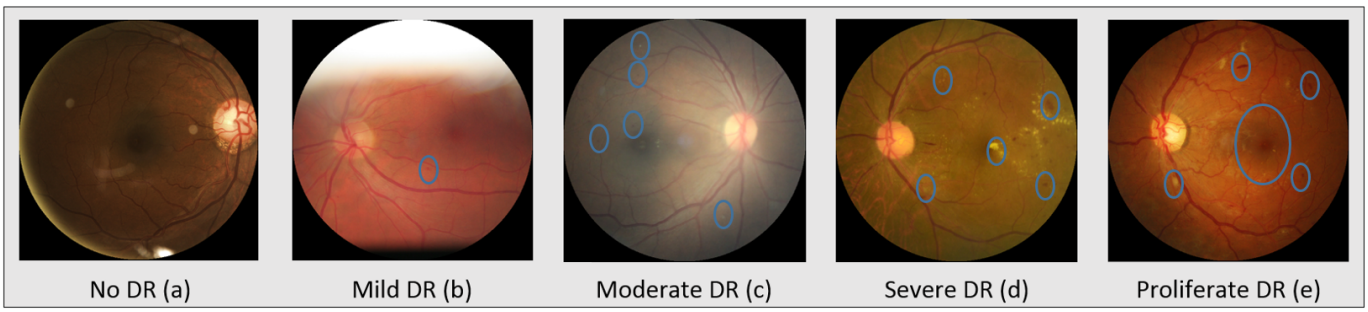

Fig. 6. Example DR images correctly classified by using HSI-LBPs, aSI-LBPs, bSI-LBPs descriptors but not by RGB-LBPs or Lab-LBP descriptors: (a) no-DR example retina image with some luminance noise; (b) example mild DR with some microaneurysm; (c) example moderate DR with multiple microaneurysms and hard exudates; (d) example severe DR with hemorrhages in 4 quadrants; (e) example proliferate DR retina image with hemorrhages, hard exudates, and fragile blood vessels around the fovea.

color spaces and color channel candidates to obtain the most discriminant LBPs features. Results of the experiments show that HSI-LBPs descriptor and its variances, a*SI-LBPs and bSI-LBPs descriptors outperform other color LBPs and gray LBPs descriptors.

For the future plan, the candidate color LBPs descriptors can be combined with features from other region or gradient detectors to improve DR performance. Other classification and ensemble techniques will be explored to achieve better accuracy.

REFERENCES

[1] Jaykumar Lachure et al., "Diabetic Retinopathy using morphological operations and machine learning," in *Advance Computing Conf. (IACC), 2015 IEEE Int.*, Banglore, 2015, pp. 617-622.

[2] Sohini Roychowdhury et al., "Dream: Diabetic retinopathy analysis using machine learning," *IEEE J. Biomedical and Health Informatics*, vol. 18, pp. 1717-1728, Dec. 2013.

[3] O. Faust et al., "Algorithms for the automated detection of diabetic retinopathy using digital fundus images: a review," *J. Medical Syst.*, vol. 36, pp. 145-157, Feb. 2012.

[4] Saiprasad Ravishankar et al., "Automated feature extraction for early detection of diabetic retinopathy in fundus images," in *IEEE Conf. Computer Vision and Pattern Recognition*, Miami, FL, 2009, pp 210-217.

[5] Wong Li Yun, et al., "Identification of different stages of diabetic retinopathy using retinal optical images," *Inform. Sci.*, vol. 178, pp. 106-121, Jan. 2008.

[6] Balint Antal and Andras Hajdu, "An ensemble-based system for microaneurysm detection and diabetic retinopathy grading," *IEEE Trans. Biomed. Eng.*, vol. 59, pp. 1720-1726, Jun. 2012.

[7] Muthu Rama Krishnan Mookiah et al., "Computer-aided diagnosis of diabetic retinopathy: A review." *Comput. in Biology and Medicine*, vol. 43, pp. 2136-2155, Dec. 2013.

[8] Thomas Walter and Jean-Claude Klein, "Segmentation of color fundus images of the human retina: Detection of the optic disc and the vascular tree using morphological techniques," in *2nd Int. Symp., ISMDA*, Madrid, Spain, 2001, pp. 282-287.

[9] Jagadish Nayak et al., "Automated identification of diabetic retinopathy stages using digital fundus images," *J. Medical Syst.*, vol. 32, pp. 107-115, Apr. 2008.

[10] Jorge de la Calleja et al., "LBP and Machine Learning for Diabetic Retinopathy Detection," in *Intelligent Data Engineering and Automated LearningIDEAL 2014*, Salamanca, Spain, 2014, pp. 110-117.

[11] Muhammad Nadeem Ashraf et al., "Texture Feature Analysis of Digital Fundus Images for Early Detection of Diabetic Retinopathy," in *11th Int. IEEE Conf. Computer Graphics, Imaging and Visualization (CGIV)*, Singapore, 2014, pp. 57-62.

[12] Chengjun Liu and Harry Wechsler, "Robust coding schemes for indexing and retrieval from large face databases," *IEEE Trans. Image Process.*, vol. 9, no. 1, pp. 132-137, Jan. 2000.

[13] Chanjira Sinthanayothin et al., "Automated localisation of the optic disc, fovea, and retinal blood vessels from digital colour fundus images," *British J. Ophthalmology*, vol. 83, no. 8, pp. 902-910, Feb. 1999.

[14] U. R. Acharya et al., "Computer-based detection of diabetes retinopathy stages using digital fundus images," in *Proc. Institution of Mechanical Engineers, Part H: J. Engineering in Medicine*, vol. 223, no. 5, pp. 545-553, Jul. 2009.

[15] K. Ram and S. Jayanthi, "Multi-space clustering for segmentation of exudates in retinal color photographs," in *2009 Annu. Int. Conf. IEEE Engineering in Medicine and Biology Society*, Minneapolis, MN, 2009, pp. 1437-1440.

[16] Jiawei Han and Micheline Kamber, "Classification and Prediction," in *Data mining: concepts and techniques*, 2nd ed., San Francisco: Morgan Kaufmann, 2006, ch. 6, pp. 285-378.

[17] Mark S. Nixon and Alberto S. Aguado, "Color images," in *Feature extraction & image processing for computer vision*, 3rd ed., London, UK: Academic Press, 2012, ch. 13, pp. 541-599.

[18] Yu-Ichi Ohta et al., "Color information for region segmentation," *Comput. Graph. and Image Process.*, vol. 13, pp. 222-241, Jul. 1980.

[19] Sugata Banerji et al., "Novel color LBP descriptors for scene and image texture classification," in *15th Int. Conf. Image Processing, Computer Vision, and Pattern Recognition*, Las Vegas, NV, 2011, pp. 537-543.

[20] P. J. Baldevbhai and R. S. Anand, "Color image segmentation for medical images using L* a* b* color space," *IOSR J. Electron. and Commun. Eng. (IOSRJECE)*, vol. 1, pp. 24-45, May 2012.

[21] T. Ojala et al., "A comparative study of texture measures with classification based on featured distributions," *Pattern recognition*, vol. 29, pp. 51-59, Jan. 1996.

[22] T. Ojala et al., "Multiresolution Gray Scale and Rotation Invariant Texture Classification With Local Binary Patterns," *IEEE Trans. Pattern Anal. Mach. Intell.*, vol. 24, pp. 971-987, Jul. 2002.

[23] Timo Ahonen, et al., "Face description with local binary patterns: Application to face recognition," *IEEE Trans. Pattern Anal. Mach. Intell.*, vol. 28, pp. 2037-2041, Dec. 2006.

[24] Ian H. Witten and Eibe Frank, "Transformations: Engineering the input and output," in *Data Mining: Practical machine learning tools and techniques*, 2nd ed., San Francisco: Morgan Kaufmann, 2005, ch. 7, sec. 3, pp. 305-311.

[25] Chengjun Liu and Harry Wechsler, "Gabor feature based classification using the enhanced fisher linear discriminant model for face recognition," *IEEE Trans. Image Process.*, vol. 11, pp. 467-476, Apr 2002.

[26] Daniel L. Swets and John Juyang Weng. "Using discriminant eigenfeatures for image retrieval," *IEEE Trans. Pattern Anal. Mach. Intell.*, vol. 18, pp. 831-836, Aug. 1996.